

NUCLEON–DEUTERON CAPTURE WITH
CHIRAL POTENTIALSR. SKIBIŃSKI^a, J. GOLAK^a, H. WITAŁA^a, W. GLÖCKLE^b, A. NOGGA^c
E. EPELBAUM^{c,d}^aM. Smoluchowski Institute of Physics, Jagellonian University
Reymonta 4, 30-059 Kraków, Poland^bInstitut für Theoretische Physik II, Ruhr-Universität Bochum
D-44780 Bochum, Germany^cInstitut für Kernphysik, Forschungszentrum Jülich
D-52425 Jülich, Germany^dHelmholtz-Institut für Strahlen- und Kernphysik (Theorie), Universität Bonn
Nußallee 14-16, D-53115 Bonn, Germany*(Received June 14, 2006)*

Present day chiral nucleon–nucleon potentials up to next-to-next-to-next-to leading order and three nucleon forces at next-to-next-to leading order are used to analyze nucleon–deuteron radiative capture at deuteron laboratory energies below $E_d \approx 100$ MeV. The differential cross section and the deuteron analyzing powers $A_y(d)$ and A_{yy} are presented and compared to data. The theoretical predictions are obtained in the momentum-space Faddeev approach using the nuclear electromagnetic current operator with exchange currents introduced via the Siegert theorem. The chiral forces provide the same quality of data description as a combination of the two-nucleon AV18 and the three-nucleon Urbana IX interactions. However, the different parametrizations of the chiral potentials lead to broad bands of predictions.

PACS numbers: 21.45.+v, 25.10.+s, 25.40.Lw

1. Introduction

Various modern (semi)phenomenological nucleon–nucleon (NN) potentials [1–3] adjusted to the nucleon–nucleon data allow for a relatively good description of few-nucleon systems. Moreover, the existing models of a three nucleon force (3NF) when combined with those potentials led generally to an improvement in the description of three and four nucleon bound states [4–7] and reactions in the 3N-continuum [8–10]. Despite indisputable successes such forces lack reliable theoretical justification in the underlying theory of

strong interactions — the quantum chromodynamics (QCD). Recently, a new family of nuclear potentials has been derived [11–14] which has a direct connection to QCD. Incorporating the spontaneously and explicitly broken chiral symmetry, which plays a fundamental role in QCD, it is possible to construct nuclear forces in the framework of chiral perturbation theory. This approach has been originally proposed by Weinberg [15] and further developed by Ordóñez *et al.* [16], Kaiser *et al.* [17], Entem *et al.* [13], and by Epelbaum *et al.* [14, 18]. (See also recent review articles [11, 12, 19] and references therein). Up to now, NN and 3N forces have been worked out and applied in few-nucleon systems up to next-to-next-to-next-to-leading order (N^3LO) and next-to-next-to-leading order (N^2LO), respectively. The leading 4N-forces have also been worked out recently [20]. The chiral forces have already been successfully used to describe the elastic nucleon–deuteron scattering [21] and the deuteron breakup processes [21, 22]. We remind the reader that applications of chiral nuclear forces are limited to the low-energy region.

Chiral effective field theory has also been used to study processes with external pions and/or photons, see [23–26] for some recent applications. While the neutron–proton radiative capture has already been considered in this framework [27], no such analysis is available for electromagnetic processes with three nucleons. In this study we would like, at least partially, to fill this gap by presenting for the first time the chiral predictions for the $n + d \rightarrow \gamma + {}^3H$ and $p + d \rightarrow \gamma + {}^3He$ processes.

We use the chiral NN potentials [14] at next-to leading order (NLO), next-to-next-to leading order (N^2LO) and at next-to-next-to-next-to leading order (N^3LO) of chiral expansion. In the N^2LO where the 3NF contributes for the first time, we also include such 3NF's [21] consistent with the two-body interaction at this order. A complete study of electromagnetic processes in the chiral effective field theory would require the usage of the nuclear electromagnetic current operator derived consistently with the applied nuclear forces. Such a current operator is, however, not yet available, see Ref. [28] for some early work along these lines. For that reason, we decided to adopt in the present study our standard approach [29], in which the electromagnetic current operator is taken in the form of a one-body current supplemented with some many-body contributions introduced via the Siegert theorem.

In Section 2 we shortly describe our theoretical formalism. Results and a comparison to data are presented in Section 3. We summarize in Section 4.

2. Theoretical formalism

The present study is based on the formalism described in detail in [29–31]. The calculations are done for the two-body photodisintegration of the 3N bound state and the nuclear matrix element for the radiative Nd-capture N_μ^{rad} is found by applying the time reversal to the photodisintegration amplitude N_μ^{Nd} . The latter one is a matrix element of the electromagnetic current operator j_μ between the initial 3N bound state $|\Psi_b\rangle$ and the final scattering state $|\Psi_{\text{Nd}}^{(-)}\rangle$

$$N_\mu^{\text{Nd}} \equiv \langle \Psi_{\text{Nd}}^{(-)} | j_\mu | \Psi_b \rangle. \quad (1)$$

In the Faddeev scheme N_μ^{Nd} can be written in the form [30]

$$N_\mu^{\text{Nd}} = \langle \psi_1 | (1 + P) j_\mu | \Psi_b \rangle, \quad (2)$$

where $|\psi_1\rangle$ is a Faddeev component of the state $|\Psi_{\text{Nd}}^{(-)}\rangle$ and P is a permutation operator defined as a sum of cyclical and anti-cyclical permutations of three particles

$$P \equiv P_{12}P_{23} + P_{13}P_{23}, \quad (3)$$

where P_{ij} interchanges the i -th and j -th nucleons.

Starting from the Schrödinger equation for the scattering state $|\Psi_{\text{Nd}}^{(-)}\rangle$ the transition amplitude can be written as

$$N_\mu^{\text{Nd}} = \langle \phi_1 | (1 + P) | j_\mu | \Psi_b \rangle + \langle \phi_1 | P | \tilde{U} \rangle, \quad (4)$$

where $|\phi_1\rangle$ is a product of the internal deuteron state and a momentum eigenstate of the free nucleon–deuteron motion. The auxiliary state $|\tilde{U}\rangle$ fulfills the Faddeev-like equation

$$\begin{aligned} |\tilde{U}\rangle = & \left(tG_0 + \frac{1}{2}(1 + P)V_4^{(1)}G_0(tG_0 + 1) \right) (1 + P)j_\mu | \Psi_b \rangle \\ & + \left(tG_0P + \frac{1}{2}(1 + P)V_4^{(1)}G_0(tG_0 + 1)P \right) |\tilde{U}\rangle, \end{aligned} \quad (5)$$

where $V_4^{(1)}$ is a part of the 3NF which is symmetrical under the exchange of nucleons 2 and 3, G_0 is the free three-nucleon propagator, and t_1 is the two-body t -operator acting in the 2–3 subspace.

Equation (5) is solved in the momentum-space basis

$$|p, q, \alpha_J\rangle = |p, q, (ls)j, (\lambda, \frac{1}{2}) I(jI)J; (t\frac{1}{2}) T\rangle, \quad (6)$$

where p and q are the magnitudes of the two Jacobi momenta. The quantum numbers l , s , and j are the two-body subsystem orbital angular momentum,

spin and the total angular momentum, respectively. The orbital angular momentum λ of the spectator nucleon together with its spin $\frac{1}{2}$ couples to the total spectator angular momentum I . The angular momenta j and I couple finally to the total angular momentum of the 3N system J . Similar coupling $(t\frac{1}{2})T$ occurs for the isospin quantum numbers.

Starting from the transition matrix element N_{μ}^{Nd} the observables follow in a standard way [31].

3. Results

The chiral potentials depend on low energy constants (LEC) and the cut-off parameters $\tilde{\Lambda}$ and Λ . The LEC's are determined for given $\tilde{\Lambda}$ and Λ from a fit to NN and 3N data. The $\tilde{\Lambda}$ cut-off appears in the spectral function regularization [18] and ensures that the high-momentum components of the two-pion exchange are explicitly excluded from the potential. The cut-off Λ comes from a further regularization of the potential as used in the Lippmann–Schwinger equation, which cuts off the (meaningless) contributions of high-momentum states in the dynamical equation. We performed numerical calculations for a few combinations of $(\Lambda, \tilde{\Lambda})$ values which covers the possible ranges of the regularization parameters: (450 (400 at NLO), 500), (600 (550 at NLO), 500 (600 at N³LO)), (550,600), (450 (400 at NLO),700), (600 (550 at NLO),700) (in units of [MeV/c]).

The theoretical predictions at a given chiral order provide a band comprising all results. The bands presented in the following correspond to the NN potential at NLO, N²LO, NN+3NF at N²LO, and finally to the NN potential at N³LO.

Let us start the presentation of our results with the c.m. differential cross section for the neutron–deuteron (Figs. 1–3) and proton–deuteron (Figs. 4–6) capture. In Fig. 1 we display predictions at incoming neutron lab. energy $E_n = 9$ MeV and 10.8 MeV. The light (cyan) band corresponds to NLO predictions while the dark (red) one refers to the full (*i.e.* NN+3NF) N²LO results. While the NLO band is relatively broad, the N²LO band is much narrower. This shows the fast convergence of the chiral expansion for this observable. The NN+3NF N²LO chiral predictions are in agreement with the AV18+Urbana IX combination of the standard NN and 3NF models obtained using the same current operator. In Fig. 2 we show a scale of 3NF effects at N²LO by comparison predictions which corresponds to the full Hamiltonian (dark band) and other ones which corresponds to the interaction restricted to the NN force only (light band). Results obtained with NN force at N²LO are similar to those at NLO. Due to the width of the NN band it is difficult to conclude if the inclusion of the 3NF improves or not the description of the data, however the 3NF effects are clear. There is

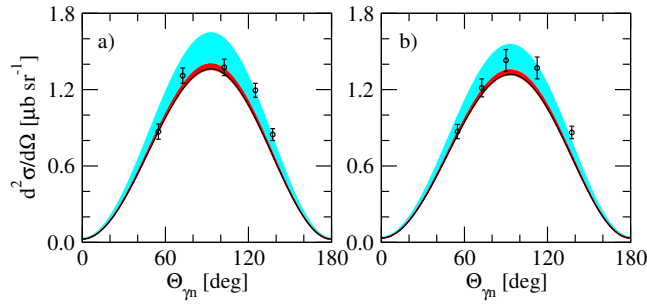


Fig. 1. The c.m. neutron–deuteron capture cross section at: 9.0 MeV (a) and 10.8 MeV (b) neutron lab. energies. The light (cyan) and dark (red) shaded bands are NN NLO and NN+3NF N²LO predictions, respectively. The solid line represents prediction obtained with the AV18 and Urbana IX forces. Data are from [32].

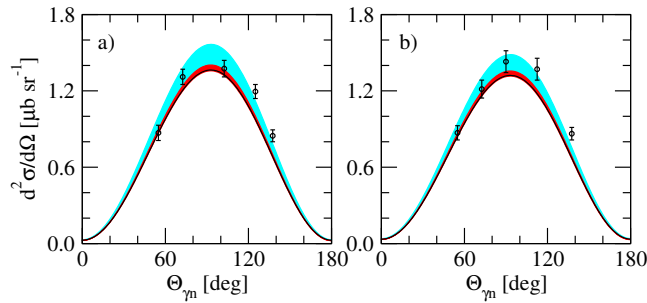


Fig. 2. The c.m. neutron–deuteron capture cross section at: 9.0 MeV (a) and 10.8 MeV (b) neutron lab. energies. The light (cyan) and dark (red) shaded bands are NN and NN+3NF force predictions at N²LO. The line and data as in Fig. 1.

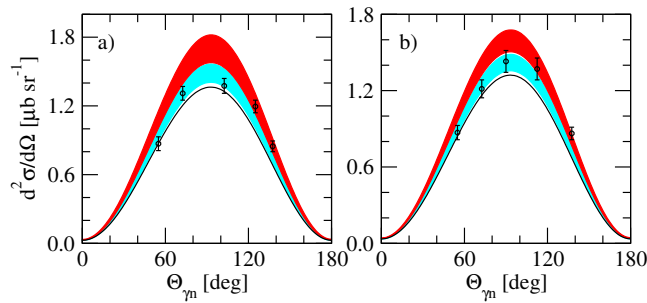


Fig. 3. The c.m. neutron–deuteron capture cross section at: 9.0 MeV (a) and 10.8 MeV (b) neutron lab. energies. The light (cyan) and dark (red) shaded bands are NN force predictions at N²LO and N³LO, respectively. The solid line and data as in Fig. 1.

an improvement at smaller $\Theta_{\gamma n}$ angles but at larger angles the data favor the pure NN predictions. The comparison between N²LO and N³LO based on NN interactions only is shown in Fig. 3. The inclusion of the additional terms appearing in N³LO (without corresponding 3NFs) shifts the predictions above those of N²LO and brings them above the data. It would be interesting to see if the inclusion of the 3NFs in N³LO will decrease the cross section bringing theory back to the data, similarly as it is the case at N²LO.

In Figs. 4–6 proton–deuteron capture cross sections are shown at two incoming deuteron lab. energies, $E_d = 29$ and 95 MeV. The nice convergence of chiral expansion is seen at both energies (see Fig. 4). In Fig. 5, at smaller deuteron energy $E_d = 29$ MeV the inclusion of the 3NF in N²LO shifts the results in the wrong direction, deteriorating the description of data. Passing to (incomplete) N³LO improves the agreement with data. At the much higher deuteron energy $E_d = 95$ MeV the 3NF acts in the opposite

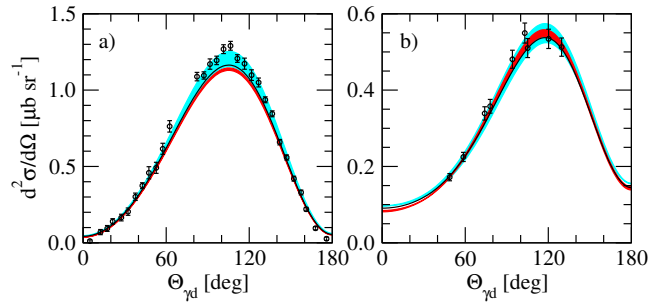


Fig. 4. The c.m. proton–deuteron capture cross section at: 29 MeV (a) and 95.0 MeV (b) deuteron lab. energies. The bands and the line as in Fig. 1. Data at 29 MeV are from [33] and at 95 MeV from [34].

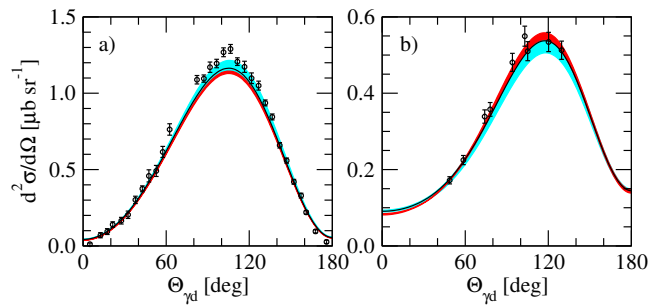


Fig. 5. The c.m. proton–deuteron capture cross sections at: 29 MeV (a) and 95 MeV (b) deuteron lab. energies. The bands and the line as in Fig. 2. Data as in Fig. 4.

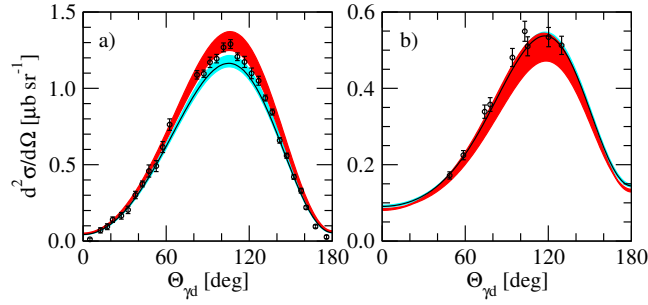


Fig. 6. The c.m. proton–deuteron capture cross sections at: 29 MeV (a) and 95 MeV (b) deuteron lab. energies. The bands and the line as in Fig. 3. Data as in Fig. 4. The wider N³LO band covers the N²LO at $E_d=95$ MeV.

direction, undoubtedly improving the data description. At this energy there is no difference between predictions at N²LO and N³LO based on the NN interactions only. However, the band of predictions at N³LO is much broader than the corresponding one at N²LO.

Now let us discuss selected spin observables. We would like to show results for the deuteron vector analyzing power $A_y(d)$ (Figs. 7–9) and the deuteron tensor analyzing power A_{yy} (Figs. 10–12) at four deuteron energies

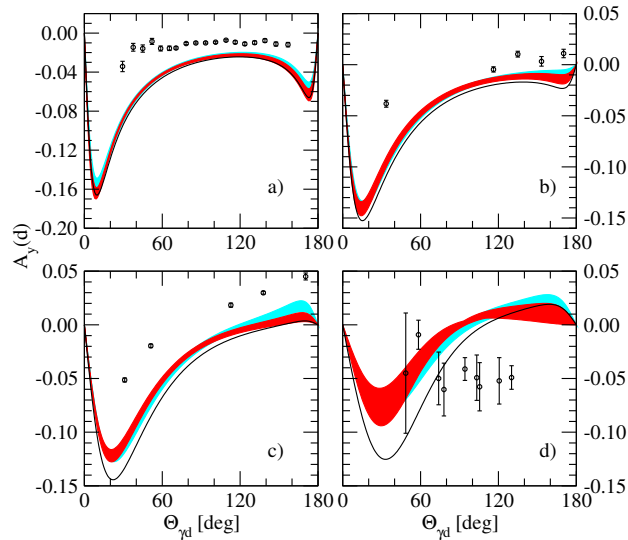


Fig. 7. The deuteron vector analyzing power $A_y(d)$ at: 17.5 MeV (a), 29 MeV (b), 45 MeV (c) and 95 MeV (d) deuteron lab. energies. The bands and the line as in Fig. 1. Data at 17.5 MeV are from [35,36], at 29 and 45 MeV from [37], at 95 MeV from [34].

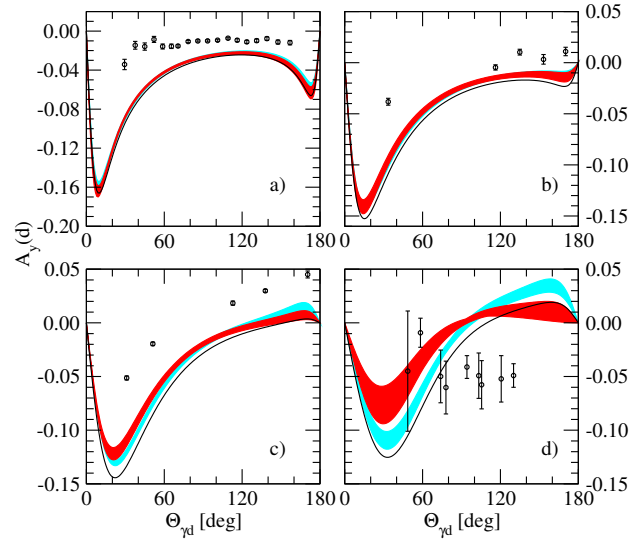


Fig. 8. The deuteron vector analyzing power $A_y(d)$ at: 17.5 MeV (a), 29 MeV (b), 45 MeV (c) and 95 MeV (d) deuteron lab. energies. The bands and the line as in Fig. 2. Data as in Fig. 7.

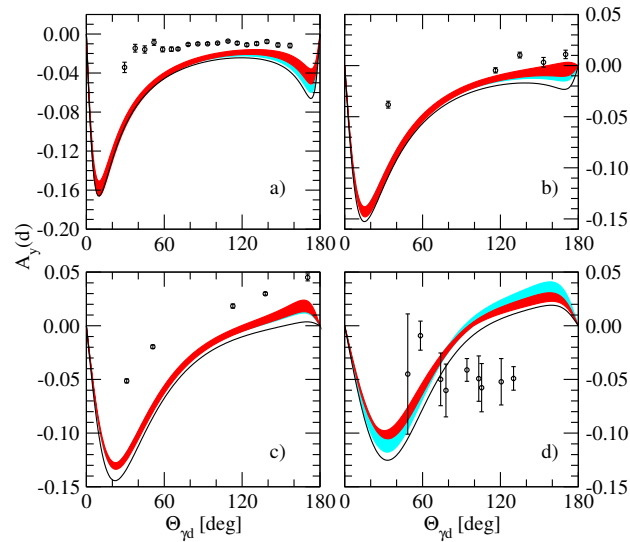


Fig. 9. The deuteron vector analyzing power $A_y(d)$ at: 17.5 MeV (a), 29 MeV (b), 45 MeV (c) and 95 MeV (d) deuteron lab. energies. The bands and the line as in Fig. 3. Data as in Fig. 7.

17.5 MeV, 29 MeV, 45 MeV and 95 MeV, for which comparison with data is possible. Here, the convergence of the chiral expansion is much slower (see Figs. 7 and 10) and the bands have more or less the same width. At the highest deuteron energy $E_d = 95$ MeV for $A_y(d)$ the N²LO band is even wider than that one in NLO. The effects of the 3NF at N²LO on $A_y(d)$ are not substantial and are seen mainly at the highest deuteron energy. The observed discrepancy with the data might at least partially be caused by the simplified model of the electromagnetic operator used in the present calculations. (The results based on the AV18+Urbana IX potential and a more realistic model of the current operator is shown in [31] where a better agreement with data was found.) The effects of the new terms occurring in the NN potential in N³LO are small, as seen in Fig. 9. At the three lower energies they slightly shift predictions in the data direction. At the highest energy the picture for $A_y(d)$ is similar when including the 3NF or the new N³LO terms. However, in the first case the band of predictions is much broader.

Similarly to the $A_y(d)$ case, the effects of moving from NLO to N²LO, as well as the 3NF effects for A_{yy} (Figs. 10–11) are not significant. The discrepancy between AV18+Urbana IX and the chiral predictions for the higher energies of 45 MeV and 95 MeV is particularly interesting. At these

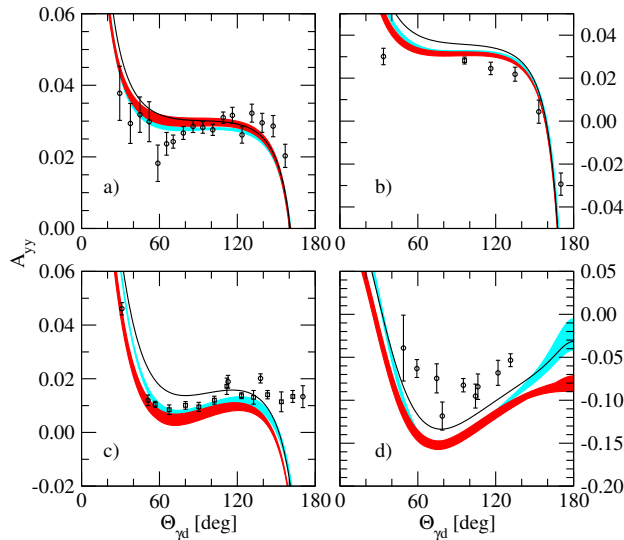


Fig. 10. The deuteron tensor analyzing power A_{yy} at: 17.5 MeV (a), 29 MeV (b), 45 MeV (c) and 95 MeV (d) deuteron lab. energies. The bands and the line as in Fig. 1. Data at 17.5 MeV from [35, 36], at 29 MeV from [38] (squares) and [37] (circles), at 45 MeV from [37] (circles) and [39] (squares) and at 95 MeV from [34].

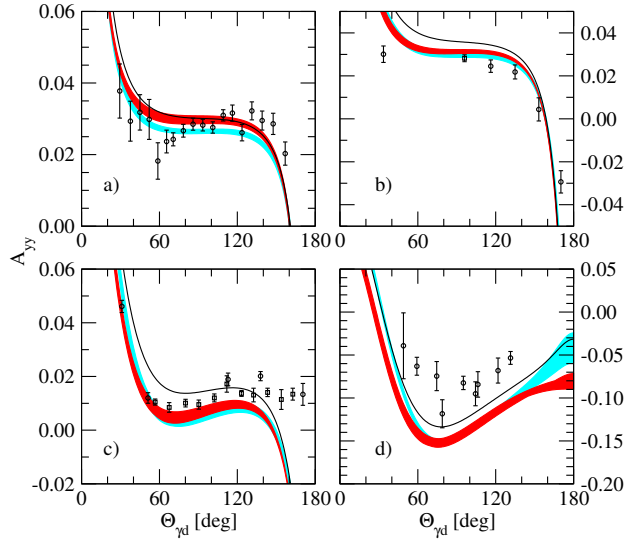


Fig. 11. The deuteron tensor analyzing power A_{yy} at: 17.5 MeV (a), 29 MeV (b), 45 MeV (c) and 95 MeV (d) deuteron lab. energies. The bands and the line as in Fig. 2. Data as in Fig. 10.

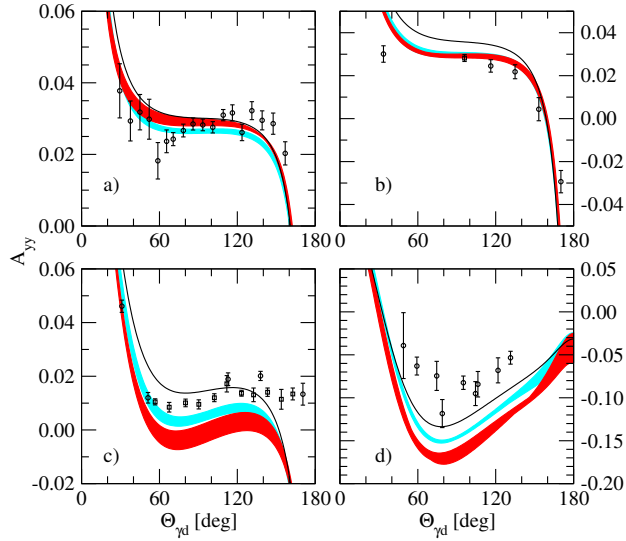


Fig. 12. The deuteron tensor analyzing power A_{yy} at: 17.5 MeV (a), 29 MeV (b), 45 MeV (c) and 95 MeV (d) deuteron lab. energies. The bands and the line as in Fig. 3. Data as in Fig. 10.

energies the step to the next order in the chiral expansion seems to be necessary (see Fig. 12). Moreover, the additional terms in the $N^3\text{LO}$ NN chiral potential shift predictions farther away from the data. This points to the need of developing the corresponding 3N forces, which is under way.

4. Summary

The first predictions for radiative nucleon–deuteron capture based on chiral forces are presented. The differential cross section and the deuteron vector and tensor analyzing powers have been calculated using the chiral NN potential at NLO, $N^2\text{LO}$ and $N^3\text{LO}$. Also the results at $N^2\text{LO}$ with the chiral 3NF of that order are shown. The nuclear current operator contains, besides the single nucleon current, some many-body contributions as introduced via the Siegert theorem. The chiral potentials give similar predictions as the AV18+Urbana IX combination of the standard nuclear forces. We found, however, a significant theoretical uncertainty for all considered observables. The bands of predictions are in some cases too broad, especially in the $N^3\text{LO}$ NN and $N^2\text{LO}$ NN+3NF cases, to make a decisive conclusion about the quality of the Nd-capture data description. This broadness can be partially caused by the inconsistent current operator used in this study. In future studies the nuclear current constructed in the same framework as chiral forces should be used. This first study indicates that the inclusion of the consistent current operator and going to $N^3\text{LO}$ in the chiral expansion might be necessary to obtain a more precise description of radiative processes within the chiral effective field theory framework. However, we have shown that already now this framework can be used for analyzing low energy electromagnetic processes.

This work has been supported by the Polish State Committee for Scientific Research (KBN) under Grant No. 2P03B00825 and by the Helmholtz Association, contract number VH-NG-222. The numerical calculations have been performed on the IBM Regatta p690+ of the NIC in Jülich, Germany.

REFERENCES

- [1] V.G.J. Stoks, R.A.M. Klomp, C.P.F. Terheggen, J.J. de Swart, *Phys. Rev.* **C49**, 2950 (1994).
- [2] R.B. Wiringa, V.G.J. Stoks, R. Schiavilla, *Phys. Rev.* **C51**, 38 (1995).
- [3] R. Machleidt, F. Sammarruca, Y. Song, *Phys. Rev.* **C53**, R1483 (1996).
- [4] J. Carlson, R. Schiavilla, *Rev. Mod. Phys.* **70**, 743 (1998).

- [5] S.C. Pieper, V.R. Pandharipande, R.B. Wiringa, J. Carlson, *Phys. Rev.* **C64**, 014001 (2001).
- [6] A. Nogga *et al.*, *Phys. Rev. Lett.* **85**, 944 (2000).
- [7] A. Nogga *et al.*, *Phys. Rev.* **C65**, 054003 (2002).
- [8] W. Glöckle, H. Witała, D. Hüber, H. Kamada, J. Golak, *Phys. Rep.* **274**, 107 (1996).
- [9] H. Witała, W. Glöckle, J. Golak, A. Nogga, H. Kamada, R. Skibiński, J. Kuroś-Żolnierczuk, *Phys. Rev.* **C63**, 024007 (2001).
- [10] J. Kuroś-Żolnierczuk, H. Witała, J. Golak, H. Kamada, A. Nogga, R. Skibiński, W. Glöckle, *Phys. Rev.* **C66**, 024003 (2002).
- [11] E. Epelbaum, *Prog. Part. Nucl. Phys.* **57**, 654 (2006) [[nucl-th/0509032](#)].
- [12] P.F. Bedaque, U. van Kolck, *Annu. Rev. Nucl. Part. Sci.* **52**, 339 (2002).
- [13] D.R. Entem, R. Machleidt, *Phys. Rev.* **C68**, 041001 (2003).
- [14] E. Epelbaum, W. Glöckle, U.-G. Meißner, *Nucl. Phys.* **A747**, 362 (2005).
- [15] S. Weinberg, *Phys. Lett.* **B251**, 288 (1990); *Nucl. Phys.* **B363**, 3 (1991); *Phys. Lett.* **B295**, 114 (1992).
- [16] C. Ordóñez, U. van Kolck, *Phys. Lett.* **B291**, 459 (1992); C. Ordóñez, L. Ray, U. van Kolck, *Phys. Rev.* **C53**, 2086 (1996).
- [17] N. Kaiser, R. Brockmann, W. Weise, *Nucl. Phys.* **A625**, 758 (1997); N. Kaiser, *Phys. Rev.* **C61**, 014003 (2000); *Phys. Rev.* **C62**, 024001 (2000); *Phys. Rev.* **C64**, 057001 (2001); *Phys. Rev.* **C65**, 017001 (2002).
- [18] E. Epelbaum, W. Glöckle, U.-G. Meißner, *Eur. Phys. J.* **A19**, 401 (2004).
- [19] S.R. Beane, P.F. Bedaque, M.J. Savage, U. van Kolck, *Nucl. Phys.* **A700**, 377 (2002).
- [20] E. Epelbaum, [nucl-th/0511025](#) to be published in *Phys. Lett. B*.
- [21] E. Epelbaum, A. Nogga, W. Glöckle, H. Kamada, U.-G. Meißner, H. Witała, *Phys. Rev.* **C66**, 064001 (2002).
- [22] St. Kistryn *et al.*, *Phys. Rev.* **C72**, 044006 (2005).
- [23] S.R. Beane, V. Bernard, E. Epelbaum, U.-G. Meißner, D.R. Phillips, *Nucl. Phys.* **A720**, 399 (2003).
- [24] S.R. Beane, M. Malheiro, J.A. McGovern, D.R. Phillips, U. van Kolck, *Nucl. Phys.* **A747**, 311 (2005).
- [25] H. Krebs, V. Bernard, U.-G. Meißner, *Eur. Phys. J.* **A22**, 503 (2004).
- [26] V. Lensky, V. Baru, J. Haidenbauer, C. Hanhart, A.E. Kudryavtsev, U.-G. Meißner, *Eur. Phys. J.* **A26**, 107 (2005).
- [27] T.S. Park *et al.*, *Phys. Lett.* **B472**, 232 (2000).
- [28] T.S. Park, D.P. Min, M. Rho, *Nucl. Phys.* **A596**, 515 (1996).
- [29] J. Golak *et al.*, *Phys. Rev.* **C62**, 054005 (2000).
- [30] R. Skibiński, J. Golak, H. Kamada, H. Witała, W. Glöckle, A. Nogga, *Phys. Rev.* **C67**, 054001 (2003).

- [31] J. Golak, R. Skibiński, H. Witała, W. Glöckle, A. Nogga, H. Kamada, *Phys. Rep.* **415**, 89 (2005).
- [32] G. Mitev *et al.*, *Phys. Rev.* **C34**, 389 (1986).
- [33] B.D. Belt, C.R. Bingham, M.L. Halbert, A. van der Woude, *Phys. Rev. Lett.* **24**, 1120 (1970).
- [34] W.K. Pitts *et al.*, *Phys. Rev.* **C37**, 1 (1988).
- [35] K. Sagara *et al.*, *AIP Conf. Proc.* **334**, 467 (1995).
- [36] H. Akiyoshi, Ph.D. thesis, Kyushu University, 1997.
- [37] T. Klechneva *et al.*, *Phys. Rev.* **C73**, 034005 (2006).
- [38] J. Jourdan, M. Baumgartner, S. Burzynski, P. Egelhof, R. Henneck, A. Klein, M.A. Pickar, G.R. Plattner, W.D. Ramsay, H.W. Roser, I. Sick, J. Torre, *Nucl. Phys.* **A453**, 220 (1986).
- [39] H. Anklin *et al.*, *Nucl. Phys.* **A636**, 189 (1998).